Lithologic characterization using magnetic and gravity gradient data over an iron ore formation in the Quadrilátero Ferrífero, Minas Gerais, Brazil

*Cericia Martinez†, Yaoguo Li†, Richard Krahenbuhl†, Marco Braga‡

† Center for Gravity, Electrical, and Magnetic Studies, Department of Geophysics, Colorado School of Mines
‡ Vale, Brazil

Abstract

Magnetic and gravity gradient data over part of the Gandarela Syncline iron formation in the Quadrilátero Ferrífero have been utilized to obtain a 3D susceptibility and density contrast model using inversion. It is possible to use these detailed 3D physical property distributions of subsurface features for lithologic interpretation purposes. We group the two physical property distributions into geologically representative units. A distribution of these lithologic units can then be organized in a model similar to the susceptibility and density distributions in order to help characterize subsurface structure.

Introduction

The combined interpretation of gravity and magnetic data has often been useful in characterizing an exploration target. With the advent of accessible systems to measure the gravity gradient, it is natural to pair gravity gradient and magnetic data for interpretation purposes where applicable.

Direct interpretation of maps aside, there has been much work in exploiting the potential field relationships to extract more information from the data. Kanasewich and Agarwal in 1970 explored the validity of examining the magnetization to density ratio in the wavenumber domain as an interpretation tool. Directly combining magnetic and gravity derived gravity gradient data in the spatial domain through the Poisson relation has been accomplished by Dransfield et. al. (1994) and Price and Dransfield (1995) in order to generate psudolithology maps based on the ratio of apparent susceptibility to density. Thanks to technological developments, gravity gradient and magnetic measurements can be made and pseudolithologic maps can be derived in a more direct manner from observed data as in Braga et. al. (2009).

Beyond direct utilization of the data to generate maps of apparent susceptibility and apparent density, inversion of the potential field data for a susceptibility and density distribution can be explored for lithologic differentiation. Lane and Guillen (2005) have explored inversion guided by lithologic categories with density and susceptibility

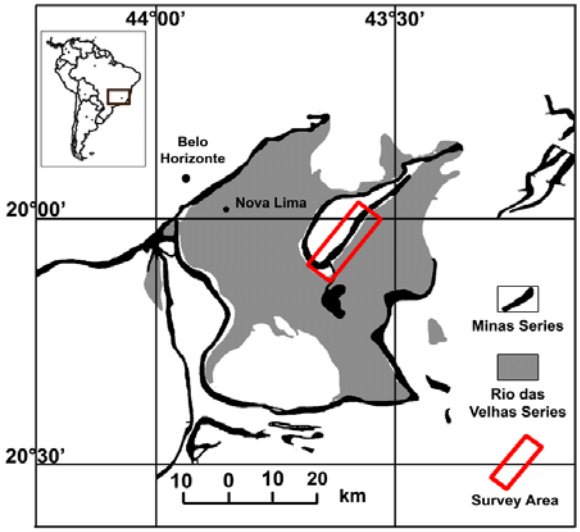

Figure 1: *Geologic map of the Quadrilátero Ferrífero, with red lines indicating where the Minas Series is present; modified from Dorr, 1965.*

properties being ancillary information. In 2007, Williams and Dipple explored estimating mineral abundance through drill data and 3D property distributions obtained by inversion of magnetic and gravity data utilizing geologic reference models.

More recently, Kowalczyk et. al. (2010) utilized 3D inversion of magnetic and gravity data to obtain regional susceptibility and density contrast models that were used to divide the region into class distributions based on a scatterplot of the physical properties.

Here, we utilize a similar approach to obtain a 3D lithologic model by combining susceptibility and density distributions obtained via inversion of magnetic and gravity gradient data.

3D Inversion of potential field data

Inversion of the magnetic data was carried out based on the methodology set forth by Li and Oldenburg in 1996 and 2003. The algorithm was then adapted for use with gravity gradiometry data by Li in 2001.

Since the magnetic and gravity gradient data share the same inverse cubic distance decay, the data can be treated similarly for the purposes of inversion. For brevity, we outline the general inversion algorithm applied to the magnetic and gravity gradiometry data. The algorithm assumes a physical property distribution of rectangular prisms with constant physical property. The model is

obtained via the inverse solution to the simplified general equation (1), where $\vec{m} = [\rho_1, \rho_2, ..., \rho_n]^T$ are the model cells, $\vec{d} = [d_1, d_2, ..., d_n]^T$ is the data, and G is the sensitivity matrix that describes the physics and geometry for each model cell.

$$G\vec{m} = \vec{d} \quad (1)$$

The inverse solution is obtained by minimizing a total objective function using Tikhonov regularization with given bound constraints according to (2) where μ is a regularization parameter, $\vec{\rho}_{\min}$ is a lower bound on the physical property, and $\vec{\rho}_{\max}$ is an upper bound on the physical property.

$$\begin{aligned} &\min \ \phi = \phi_d + \mu\phi_m \\ &s.t. \ \vec{\rho}_{\min} \le \vec{\rho} \le \vec{\rho}_{\max} \end{aligned} \quad (2)$$

The data misfit is defined as (3) where $\vec{d}_{obs}$ is the observed data, $\vec{d}_{pre}$ is the predicted data, and W_d is a data weighting matrix that contains information about the noise in the data.

$$\phi_d = \left\| W_d \left(\vec{d}_{obs} - \vec{d}_{pre} \right) \right\|^2 \quad (3)$$

The model objective function is defined as (4).

$$\begin{aligned} \phi(m) = &\iiint_V \left[w(z)(\vec{m} - \vec{m}_0) \right]^2 dv \\ &+ L_x^2 \iiint_V \left[\frac{\partial w(z)(\vec{m} - \vec{m}_0)}{\partial x} \right]^2 dv \\ &+ L_y^2 \iiint_V \left[\frac{\partial w(z)(\vec{m} - \vec{m}_0)}{\partial y} \right]^2 dv \\ &+ L_z^2 \iiint_V \left[\frac{\partial w(z)(\vec{m} - \vec{m}_0)}{\partial z} \right]^2 dv \end{aligned} \quad (4)$$

Where L_x, L_y, L_z are length scales defining the relative smoothness of the resulting model in each of the Cartesian directions. The sought model is denoted by $\vec{m}$ and $\vec{m}_0$ is a reference model. The function $w(z)$ is a weighting function of the form $w(z) = (z + z_0)^{-3/2}$ used to counteract the decay of the kernel function and prevent the accumulation of density or susceptibility occurring at shallow depths. A logarithmic barrier method utilizing the conjugate gradient technique is implemented to constrain the resulting model according to user-specified bounds. The final objective function to be minimized has the form given in (5) where λ is a barrier parameter and $p_j^{\min}$ and $p_j^{\max}$ are the lower and upper bounds, respectively, on a single cell j for the unknown physical property p_j.

$$\phi(\lambda) = \phi_d + \mu\phi_m - 2\lambda \sum_{j=1}^{M} \left[\ln\left(\frac{p_j - p_j^{\min}}{p_j^{\max} - p_j^{\min}} \right) + \ln\left(\frac{p_j^{\max} - p_j}{p_j^{\max} - p_j^{\min}} \right) \right] \quad (5)$$

The utility of wavelet compression of the sensitivity matrix enables the algorithm to invert large-scale potential field data.

Field Site

The Quadrilátero Ferrífero, or Iron Quadrangle, is an area of significant mineral resources in the state of Minas Gerais, Brazil. Iron and gold are just a few mineral resources that have historically been produced from the Quadrilátero Ferrífero region (Dorr, 1969). The Quadrilátero Ferrífero covers approximately 7,000 km^2. The area has rugged terrain with canyons, plateaus, and valleys composing the landscape. The climate is semitropical with an average annual rainfall of nearly 250 cm.

Dorr (1969) gives a detailed description of the stratigraphy of the Quadrilátero Ferrífero in general and the structure of interest, the Gandarela Syncline. The iron bearing formation occurs within the Minas Series, which is composed of metasedimentary rocks thought to be Precambrian in age. The Minas Series is characterized by folding structures and is present today in regional synclinal features such as the Gandarela Syncline. The structurally controlled occurrence of the Minas Series is shown in Figure 1. The eastern flank of the Gandarela syncline has been overturned while the western flank remains upright.

Within the Minas Series, the Cauê Itabirite hosts the majority of the iron mineralization and is sandwiched between the overlying Gandarela Formation and underlying Batatal formation. The Cauê Itabirite averages 300-500 m in thickness, but can range from a few meters to over 1400 m. Generally, the deposits occur near faults and fold zones characterized by low pressure and high permeability that allow for the movement of fluids. Canga protects iron formation on ridgelines, which is a cemented, iron-formation derived layer resistant to chemical and mechanical weathering (Dorr, 1969).

Details on the structural occurrence and properties of the iron ore bodies are given by Dorr (1965). The ore bodies tend to be shallow and can range anywhere from 25 to 150 m below the surface. The ore deposits follow the structure of the host formation and are generally tabular and dipping southeast with an approximate dip of 25°. The contact between the ore and host itabirite can be gradational or feathery in nature, but is usually abrupt. The high-grade ore typically contains an average of 66% Fe with the intermediate grade ores containing an average of 63% Fe. The high-grade deposits are easily differentiated from the dolomitic and quartz-rich country rock by the stark density contrast. The host rocks contain average densities close to the typical 2.67 g/cc, while target ore densities can range from 3 g/cc to 5 g/cc.

Gravity Gradient Data

The gravity gradient data were collected in August-September 2005 in the Quadrilátero Ferrífero. The 93 km^2 survey was acquired with 100 m line spacing trending

northeast-southwest at roughly 32 degrees from the north. Only a subset of the collected dataset is presented here and covers approximately a 4 km by 5 km area.

The gravity gradient survey was semi-draped and has flight heights ranging from 60 to 500 m above the ground surface. The acquired data underwent routine proprietary processing and corrections for the centripetal force and self-gradient, acceleration compensation, and demodulation by the acquisition company. Before data delivery, the lines were leveled and filtered to attenuate noise.

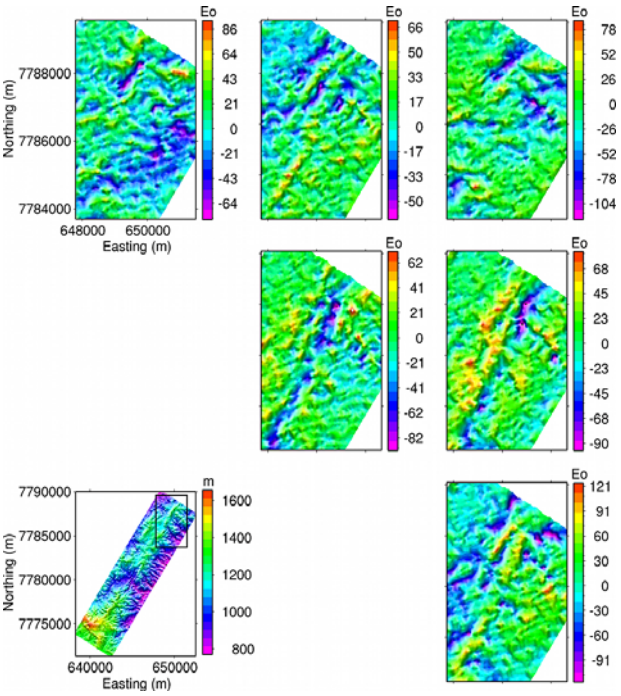

Figure 2: *Observed gravity gradient data, with lower left plot showing topography of the entire survey area and location of subset data.*

Each measured component contains information about the iron source body and has the potential to contribute to further characterizing the target ore body. Though the gravity gradient satisfies Laplace's equation and there are only five independent components, six components were measured within this survey area. The density contrast model shown in the results section was obtained by inverting six measured gravity gradient components.

The extracted data are shown in Figure 2. The geologic feature of interest, the Gandarela Syncline, runs through the middle of the data parallel to the long axis of the survey area. The topography of the entire survey area is shown in the bottom left plot with the subset location indicated by the black box. The iron formation is coincident with topographic highs in the area, making the density value used to remove the terrain effect an important parameter. To obtain the displayed gradient anomaly of Figure 2, a density value of 2.67 g/cc was used to acceptably remove the terrain effect.

Magnetic Data

The total field magnetic data was collected at the same time as the gravity gradient data, with many of the same survey parameters. The acquisition took place between August-September 2005 over the same area. The survey was acquired with 100 m line spacing trending northeast-southwest at roughly 32 degrees from the north. The same 20 km^2 subset area is used for the study here.

Three tie lines were flown over the 93 km^2 survey. The flight was smoothly draped with a nominal flight height of 100 m. Lines were oriented parallel to the topographic surface to allow for smoother adjustments to terrain clearance. Prior to delivery, the service company applied a parallax correction, height correction, removed the diurnal variation, and removed the International Geomagnetic Reference Field. The magnetic observations were upward and downward continued to maintain a constant terrain clearance of 250 m.

To prepare the magnetic data for inversion, the data was leveled and gridded at 20 m spacing. The data subset used for inversion after removal of the regional field is shown in Figure 3.

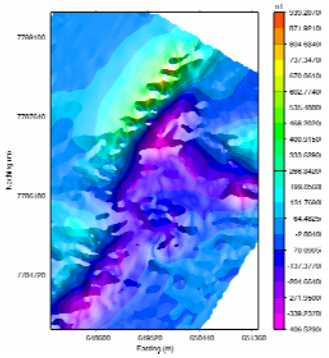

Figure 3: *Magnetic anomaly data over the same subset area as the gravity gradient data after regional-residual separation.*

Density contrast model

The gravity gradient data was inverted utilizing the inversion algorithm previously described. Six measured components (T_{xx}, T_{xy}, T_{xz}, T_{yy}, T_{yz}, and T_{zz}) were simultaneously inverted to obtain a representative density contrast model of the target subsurface geology (Martinez et. al., 2010).

The mesh is composed of rectangular prisms or cells with constant density contrast within each cell. The discretization mesh has cell sizes of 25 m in the easting by 25 m in the northing by 20 m in depth in the central region of the mesh, with padding cells beyond the data area and at large depth. The rectangular mesh has dimensions of 156 cells in the easting by 241 cells in the northing by 45 cells in depth giving a total of 1,691,820 cells. The topographic surface is implemented within the inversion, leaving only 979,443 cells after removal of cells above the topography.

The density contrast model was obtained by blind inversion of the 18,102 data points. Generic inversion parameters were used with little a priori information incorporated into the inversion. A zero reference model was used with an initial model of 2.0 g/cc. Lower and upper bounds on the density contrast were set as 0.0 g/cc and 4.0 g/cc using the knowledge that a positive density contrast is expected from the dense ore body in the less dense host rock. The length scales in each direction are two times the cell size such that $L_x = L_y = 50$ m and $L_z = 40$ m, requiring an equal amount of feature elongation in each direction. A volume rendered image of the density contrast distribution is shown in Figure 4 with model cells below 1.0 g/cc removed for clarity.

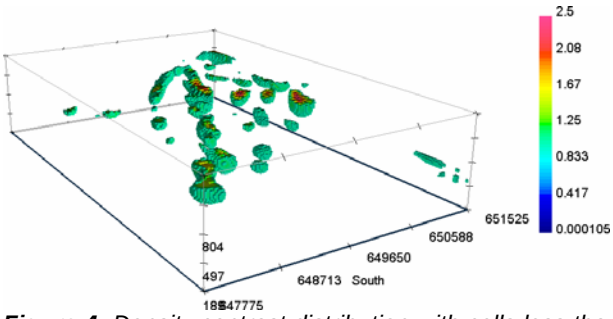

Figure 4: *Density contrast distribution with cells less than 1.0 removed; units are g/cc. Distance is in meters.*

Susceptibility model

Prior to obtaining the susceptibility model used for the lithologic model shown here, removal of the regional field was a necessity. Removal of the regional field took place by implementing an inversion methodology.

A subset of the magnetic data was inverted using a coarse mesh with cell sizes of 250 m in the easting, 250 m in the northing, and 100 m in depth.

Using generalized cross validation, a susceptibility model was obtained that explains the regional trends in the entire dataset. Since the geologic feature of interest lies near surface, the coarse 250 m by 250 m by 100 m blocks are insufficient to capture the variations with the desired detail. From the coarse regional model, we set all the cells between the topographic surface and an elevation of 919 m within the area of interest to zero and forward model the magnetic anomaly in the area of interest resulting from the remaining regional sources. The data calculated from this altered susceptibility model is now considered the regional trend that we wish to remove from the data in order to obtain the response of the near surface geology.

The regional trend is subtracted from the observed data and we use this residual magnetic data within the area of interest shown in Figure 3 to obtain a shallow, near surface susceptibility model. The mesh discretization used for the shallow model is the same as that of the gravity gradient mesh detailed earlier.

The susceptibility contrast model was obtained by blind inversion of the 12,037 data points. A zero reference model was used with an initial model of 0.001 (SI). Lower and upper bounds of 0.0 and 1.0 were placed on the model to keep the recovered values within a reasonable range of susceptibilities. Coefficients that control the smoothness derivative in each direction were 0.0001 for the smallest model and 1.0 for the easting, northing, and vertical directions. A volume rendered image of the recovered susceptibility distribution is shown in Figure 5 with model cells below 0.15 (SI) removed for clarity.

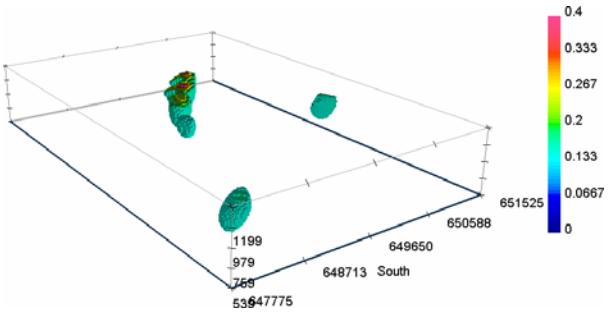

Figure 5: *Susceptibility distribution with cells less than 0.15 removed; units are SI. Distance is in meters.*

Lithologic Mapping

Now that we have obtained a density and susceptibility model, it is possible to examine the correlation that the two physical properties have with each other. A cross-plot of the corresponding model cells susceptibility versus density is generated in order to assign lithologic units based on these rock properties. Lithology types are then assigned based on the susceptibility and density values according to generally known rock properties. General density and susceptibility values for rock types were taken from Ahrens (1995).

A cross-plot for the susceptibility and density model described above is shown in Figure 6. The background density of 2.67 g/cc was added back into the density contrast model to restore the original density range. Note that reference is made to the density contrast model. The cross-plot is characterized by a dense region of low susceptibilty, low density values. In addition, we see finger-like clusters extending outward from the main cloud of points.

We next assign colors to collections of points within the cross-plot to better visualize the relationships. With these color assignments, we are then able to generate a 3D model to see the lithologic representations. The geologic section given in Figure 7 provides information for evaluating our lithologic assignments. A cross section through our constructed lithologic model, corresponding to the geologic section of Figure 7, is shown in Figure 8. For consistency, we have maintained the same color scheme for the lithologic units in the cross plot and the lithologic model. For additional comparison, the corresponding cross section from the separate density contrast and susceptibility models are shown in Figures 9 and 10, respectively. From the susceptibility, density, and lithologic models it is observed that the high density iron ore within the Caue Itabirite is identified by low susceptibility in general.

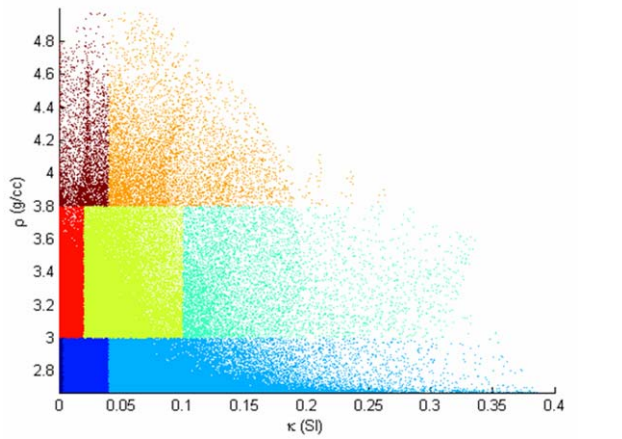

Figure 6: *Cross-plot of susceptibility model versus density with lithologic units color coded.*

A cursory look at the cross sections in Figures 8 – 10 may result in the conclusion that density range assignments from the cross-plot are more relevant than susceptibility. This is because the dominant features within the lithologic section (Figure 8) are largely consistent with the density contrast model (Figure 9). However, this conclusion is not accurate, and such an assumption can lead to a gross overestimate of total ore volumes. To demonstrate, we first direct our attention to the full 3D lithologic volume that the cross section of Figure 8 was extracted from. A volume rendered image of this model is given in Figure 11, and all of the lithologic units have been removed except for the one corresponding to hematite (maroon in both the upper left part of the cross-plot, and in Figure 8). When we incorporate both density and susceptibility constraints on the lithologic model, as we have done here, the result is a distribution consistent with known hematite from drill records.

For comparison, we next remove the susceptibility constraints on the hematite, and thus define the lithologic unit based solely on the upper and lower bounds from density. This alternate scenario corresponds to the cross-plot in Figure 12, where maroon denotes hematite with no susceptibility constraints. The volume rendered image of the resulting 3D lithologic model is shown in Figure 13, as before, with all units removed except the one corresponding to hematite (maroon). The structure of the overall lithologic model (Figure 13) is similar to the recovered density contrast volume (Figure 4). However, knowledge of the site's geology indicates that the total hematite volumes may be significantly overestimated in this instance. Therefore, both recovered density and susceptibility constraints are required to generate a 3D lithologic model of the site.

Conclusions

Susceptibility and density models have been generated from airborne magnetic and gravity gradient data in the Quadrilátero Ferrífero. With the computational power of today's desktop computer, it is possible to obtain models of local subsurface detail for interpretation purposes. As a means of further utilizing inversion for interpretation on a local rather than regional scale, it is possible to combine physical property models. The two physical property distributions can be grouped into geologically representative units. These lithologic units can then be organized in a model similar to the susceptibility and density distributions in order to help characterize subsurface structure.

Utilizing inverse models has the potential to be a powerful interpretation tool, particularly combined with other general geologic information. Preliminary models such as the susceptibility distribution, density distribution, and lithologic character may prove useful in planning further exploration in both greenfield and brownfield type areas.

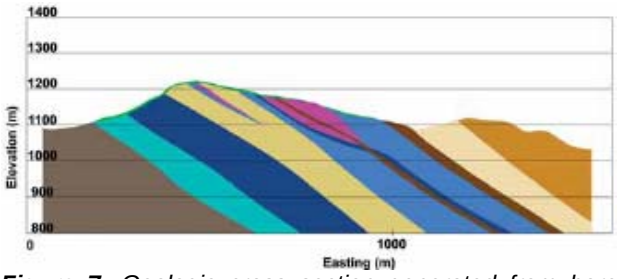

Figure 7: *Geologic cross section generated from bore hole data showing itabirite in blue and hematite in pink*

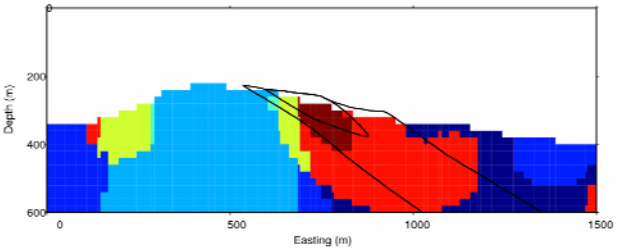

Figure 8:*.Cross section through lithologic model corresponding to geologic section of Figure 8 and color scheme identified in cross plot.*

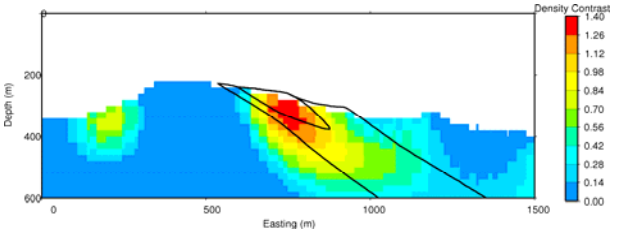

Figure 9: *Cross section through density contrast model corresponding to geologic cross section of Figure 7; units are g/cc.*

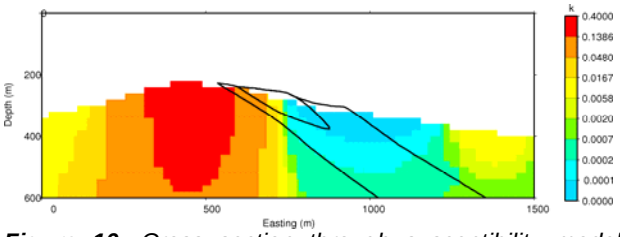

Figure 10: *Cross section through susceptibility model corresponding to geologic cross section of Figure 7 plotted on a logarithmic scale; units are SI.*

Acknowledgments
Thanks to Misac Nabighian for assisting in magnetic data reduction. We thank the sponsors of the Gravity and Magnetics Research Consortium (GMRC) for supporting this work: Anadarko, BP, BGP, ConocoPhillips, Fugro, Marathon Oil, Petrobras, and Vale.

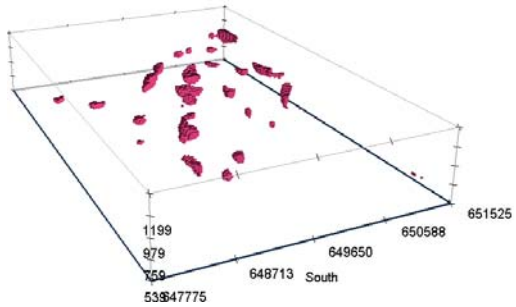

Figure 11: *Hematite distribution with density and susceptibility constraints applied from Figure 6 cross-plot.*

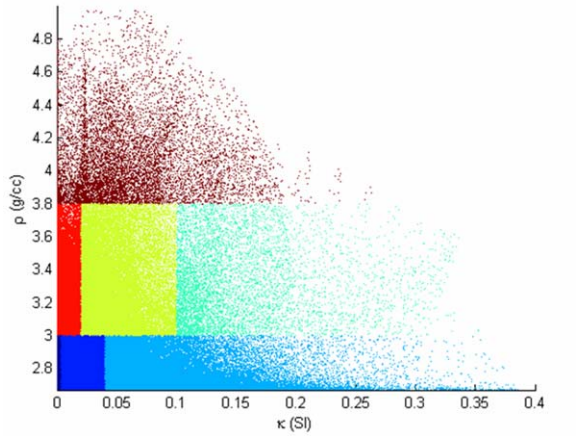

Figure 12: *Cross-plot of susceptibility model versus density with no constraints on hematite susceptibility.*

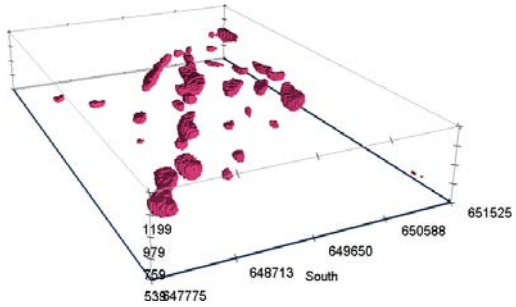

Figure 13: *Overestimate of hematite distribution when no susceptibility constraints are applied; from cross-plot in Figure 12.*

References

Ahrens, T.J., 1995, Rock Physics & Phase Relations, A Handbook of Physical Constants: American Geophysical Union.

Braga, M.A., D.U. Carlos, T. Almeida, H. Dayan, R.R. Sousa, and C.A. Braga, 2009, Mapeamento litológico por correlação entre dados de aeromagnetometria e aerogradiometria gravimétrica 3D-FTG no Quadrilátero Ferrífero, Minas Gerais, Brasil: Revista Brasileira de Geofísica, 27, 255-268.

Dorr, J. V. N., 1965, Nature and origin of the high-grade hematite ores of Minas Gerais, Brazil: Economic Geology and the Bulletin of the Society of Economic Geologists, 60, no. 1, 1–46.

Dorr, J. V. N., 1969, Physiographic, stratigraphic and structural development of the Quadrilátero Ferrífero Minas Gerais, Brazil: U.S. Government Printing Office:

Dransfield, M.H., M.J. Buckingham, and F.J. van Kann, 1994, Lithological Mapping by Correlation Magnetic and Gravity Gradient Airborne Measurements: Exploration Geophysics, 25, 25-30.

Kanasewich, E.R., and R.G. Agarwal, 1970, Analysis of Combined Gravity and Magnetic Fields in Wave Number Domain: Journal of Geophysical Research, 75, 5702-5712.

Kowalczyk, P., D. Oldenburg, N. Phillips, T.N. Hai Nguyen, and V. Thomson, 2010, Acquisition and Analysis of the 2007-2009 Geoscience BC airborne data: Australian Society of Exploration Geophysicists – PESA Airborne Gravity Workshop.

Lane, R., and A. Guillen, 2005, Geologically-inspired Constraints for a Potential Field Litho-inversion Scheme: Proceedings of IAMG: GIS and Spatial Analysis, 181-186.

Li, Y., and D.W. Oldenburg, 1996, 3-D inversion of magnetic data: Geophysics, 61, 394-408.

Li, Y., 2001, 3-D inversion of gravity gradiometer data: SEG Technical Program Expanded Abstract, 20, 1470–1473.

Li, Y. and D.W. Oldenburg, 2003, Fast inversion of large-scale magnetic data using wavelet transforms and logarithmic barrier method, Geophysical Journal International, 152, 251-265.

Martinez, C., Y. Li, R. Krahenbuhl, M. Braga, 2010, 3D Inversion of airborne gravity gradiometry for iron ore exploration in Brazil: SEG Technical Program Expanded Abstract, 29, 1753-1757.

Price, A.D., and M.H. Dransfield, 1995, Litholgical Mapping by Correlation of the Magnetic and Gravity Data from Corsair W.A.: Exploration Geophysics, 25, 179-188.

Williams, N., and G. Dipple, 2007, Mapping Subsurface Alteration Using Gravity and Magnetic Inversion Models: Proceedings of the Fifth Decennial International Conference on Mineral Exploration, 461-472.